Materials Today Communications 33 (2022) 104676

Contents lists available at ScienceDirect

Materials Today Communications

journal homepage: www.elsevier.com/locate/mtcomm

Microstructure evolution and static recrystallization kinetics in hot-deformed austenite of coarse-grained Mo-free and Mo containing low-carbon CrNiMnB ultrahigh-strength steels

Mohammed Ali [a,b,*], Oskari Seppälä [a], Timo Fabritius [c], Jukka Kömi [a]

[a] Materials and Mechanical Engineering, Centre for Advanced Steel Research, University of Oulu, P.O. Box 4200, FI-90014 Oulu, Finland
[b] Steel Technology Department, Central Metallurgical Research and Development Institute, Helwan 11421, Egypt
[c] Process Metallurgy Research Unit, Centre for Advanced Steel Research, University of Oulu, P.O. Box 4300, FI-90014 Oulu, Finland

ARTICLE INFO

Keywords:
Static recrystallization
Stress relaxation
Thermomechanical processing
Ultrahigh strength steels
Grain growth
Kinetic model

ABSTRACT

The static recrystallization characteristics and microstructure evolution in hot-deformed austenite were evaluated for a newly developed low-carbon CrNiMnB ultrahigh-strength steel with and without molybdenum addition. The time for 50% static recrystallization ($t_{50\%}$) over a wide range of strains and hot-deformation temperatures were obtained using the stress-relaxation technique on Gleeble thermomechanical simulator. Moreover, effect of deformation parameters on the size distribution and average size of prior austenite grains are investigated. A novel semi-automatic stress relaxation test reading tool with a graphical user interface was created and used successfully for the current study. The obtained results of strain's power and the apparent activation energy are within the range stated in literature for C-Mn and microalloyed steels. Addition of molybdenum increase the power of strain and the apparent activation energy from − 1.9 to − 2.6 and 206 to 212 kJ/mol, respectively. The retardation effect of molybdenum addition was shown by a new regression equation devised for calculating $t_{50\%}$. The developed equations show a good agreement with the experimental data and can be used in the designing of roughing during thermomechanical processing. The deformation parameters i.e., temperature, strain and holding time have a significant effect on the size distribution and average size of prior austenite grains.

1. Introduction

The final microstructure of thermomechanically-processed steels is determined by the recrystallization behavior of austenite. Dynamic, static, and meta-dynamic recrystallization have been postulated as the three most common recrystallization processes. Under various processing circumstances, each of these can have an impact on microstructural development [1]. Control of hot rolling in the recrystallization regime i.e., above the no-recrystallization temperature (T_{nr}) is beneficial for the refinement of austenite grain size prior to phase transformation. Therefore, static recrystallization (SRX) is the primary mechanism in most commercial hot deformation techniques [1,2] which can alter the grain characteristics i.e., size and distributions in metals and alloys [3]. In hot deformation process, SRX normally happens during the interval time, and it involves nucleation and growth processes of new grains, which require enough time to occur that could be less than one second or hundreds of seconds depending on the chemical composition, strain, and temperature. The SRX kinetics are affected by the processing factors such as strain rate, deformation temperature, and strain. A coarser initial grain size and strain induced precipitation retard the SRX process [4].

Extensive research has been conducted on the impact of alloying elements on the SRX kinetics of hot-deformed austenite. In general, as alloy content increases, SRX gets slower due to the segregation of alloying element on the dislocation and grain boundaries, however there are significant variances in the capabilities of different alloying elements [5–9]. Furthermore, the presence of a synergetic impact between the alloying elements results in a greater retarding effect than would be expected based on the sum of the separate additions [10]. At high temperature, the SRX kinetics are slowed by alloying due to a decrease in grain boundary mobility, which is related to solute drag. Generally, the solute drag strength is related to the atomic mismatch between gamma-iron and the alloying element. However, elastic modulus and

* Corresponding author at: Materials and Mechanical Engineering, Centre for Advanced Steel Research, University of Oulu, P.O. Box 4200, FI-90014 Oulu, Finland.
E-mail address: mohammed.ali@oulu.fi (M. Ali).

https://doi.org/10.1016/j.mtcomm.2022.104676
Received 21 June 2022; Received in revised form 31 August 2022; Accepted 10 October 2022
Available online 13 October 2022

electronic differences might also be factors [11]. At low temperature, the grain boundary mobility is decreased by the strain induced precipitates i.e., carbides and/or nitrides [11].

Pereda et al. [12] studied the effect of Mo on Nb-microalloyed steels with the aim of decreasing the level of Nb in the case of thin slab direct rolling to decrease the risk of precipitation of Nb(C,N) at the early stage of rolling. Addition of Mo increases the non-recrystallization temperature by about 40 °C compared to the Mo free Nb-containing steel as well as increase the retardation effect of recrystallization due to its solute drag effect [12].

Stress relaxation is a well-known and widely utilized technique for studying recrystallization in hot deformed austenite. It offers advantages over traditional double-hit approaches, including the ability to obtain a complete recrystallization percentage vs. time curve from a single test and the ability to distinguish static recovery from static recrystallization. Several double-hit experiments are required to acquire comparable results, although it is difficult to discern between static recovery and static recrystallization. Detailed description of the stress relaxation technique is given in [13]. One possible way is with the method presented by Karjalainen & Perttula (K&P) [14], as seen in Fig. 1. First, the compression and relaxation parts of the stress-time curve are separated from each other, and the relaxation start point is set to 0 s. Next the relaxation curve is studied to find an approximate time where recrystallization starts and ends. Two lines are fitted with Eq. (1) to represent the effect of recovery and grain growth, depicted by the purple and orange solid lines respectively in Fig. 1b). Then the recrystallized fraction of steel can be calculated by Eq. (2).

$$\sigma_x = \sigma_i - \alpha_i \log t \tag{1}$$

$$X = \frac{\sigma_1 - \alpha_1 \log t - \sigma(t)}{(\sigma_1 - \sigma_2) - (\alpha_1 - \alpha_2)\log t} \tag{2}$$

where t is time, σ is the present stress level and $\sigma_1,\ \ \alpha_1$ are fitting constants for the recovery and σ_2, α_2 fitting constants for the grain growth stage equations. The K&P fitting line in Fig. 1c) is created with Eq. (2).

This experimentally obtained K&P recrystallization curve is used in this study in conjunction with the Kolmogorov-Johnson-Mehl-Avrami (KJMA) equation, which is commonly used in literature to express the static recrystallized fraction (X) of steel as a function of holding time (t) [15–17]. The KJMA Eq. (3) is fitted to the K&P equation results.

$$X = 1 - \exp(-kt^n) \tag{3}$$

Where t is time, k is a fitting constant and n is the Avrami (KJMA) exponent that represents the dependency of recrystallized fractions on the nucleation and growth rate of new grains [18]. The KJMA fitting line, the blue line, in Fig. 1c) is created with Eq. (3).

An alternative method to study the recrystallization is the Zurob model, presented originally in [19] and slightly modified by Pohjonen et al. in [20]. Equation details are presented in the mentioned articles, but the basic idea is that the model is physically based and considers the effect of recovery as a dislocation density dissipation mechanism, whereas in the K&P equation recovery is just a hand-fitted line. In Fig. 1b), the green solid line is the fitted recovery line obtained by the Zurob model. Stress relaxation due to grain growth is depicted by the orange solid line described earlier. Fitted relaxation stress is the red solid line. The resulting relaxation kinetics curve is the red line in Fig. 1c).

The following empirical relation [2,5] can be used to explain $t_{50\%}$:

$$t_{50\%} = A \quad \varepsilon^p \dot{\varepsilon}^q d^s \exp\left(\frac{Q_{app}}{RT}\right) \tag{4}$$

where A, p, q and s are material dependent constants, ε is strain, $\dot{\varepsilon}$ is strain rate, d is initial grain size and Q_{app} is the apparent activation energy of static recrystallization. R is the universal gas constant and T is the absolute temperature. The recrystallized fraction may be estimated as a function of temperature and time using $t_{50\%}$ in conjunction with the KJMA equation [21].

In the current study, the effect of Mo on the static recrystallization characteristics and microstructure evolution in hot-deformed austenite were evaluated using interrupted stress relaxation technique on a Gleeble 3800 thermomechanical simulator for low-carbon CrNiMnB ultrahigh-strength steel. The effect of deformation parameters i.e., strain and deformation temperature on the static recrystallization kinetics were studied. A novel semi-automatic stress relaxation test reading tool with a graphical user interface (GUI) was created to automate as many steps as possible. Moreover, it can be used to overcome the difficulties in determination of the onset of static recrystallization manually from the

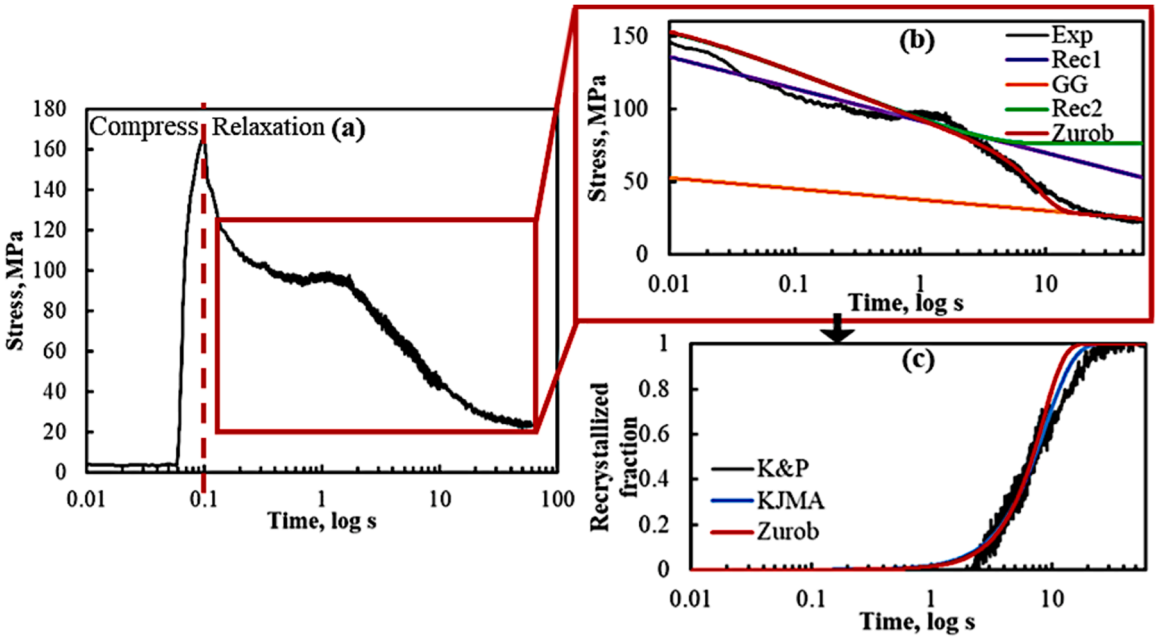

Fig. 1. A stress relaxation test result and several techniques for estimating SRX kinetics, a) full result of a relaxation test, b) relaxation part with fitted guidelines and c) calculated recrystallization kinetics.

stress relaxation curves, especially at high temperatures. SRX kinetics equations were derived for explaining static recrystallization in hot-deformed austenite of 0Mo and 0.25Mo steels. A comparison between the experimental and the predicted values using the developed SRX kinetics equations was performed. The GUI tool and fitting details are presented in appendix A. The GUI tool with example files can be found at [22].

2. Materials and methods

2.1. Materials

The chemical compositions of the investigated ultrahigh-strength steels are given in Table 1. The investigated steels have similar composition except the content of Mo. 0Mo steel refers to the steel without addition of Mo (0 wt% Mo) while 0.25Mo steel refers to the steel with addition of 0.25 wt% of Mo. The non-recrystallization (T_{nr}) temperature and the dissolution temperature for the investigated steels are given in Table 1. The materials were received in the form of homogenized and hot-rolled 12 mm-thick plates. Several rods with dimensions of 12 × 12×15 mm were cut from a hot-rolled plate with an axis parallel to the rolling direction. The rods were homogenized at 1250 °C for 1 hr. under argon atmosphere then quenched in water. Cylindrical specimens of dimensions Ø10 × 12 mm were machined from the rods with axis along with the rolling direction.

2.2. Thermomechanical simulation

Gleeble 3800® (Dynamic Systems Inc., Poestenkill, NY, USA) thermomechanical simulator was employed for interrupted stress relaxation testing. A graphite foil was used as a lubricant between the sample and the tungsten carbide anvils and tantalum foil to prevent sticking. The samples were heated at 10 °C/s to 1250 °C and held for 120 s for homogenization and increase the grain size then cooled at 2 °C/s to the deformation temperature where samples hold for 15 s prior compression up to the prescribed strain as shown in Fig. 2. Using the stroke mode, the strain was held constant after the deformation and the compression force relaxed as a function of holding time, and the stress relaxation curve fitted with an Avrami-type (KJMA) equation and Zurob fitting model for determining $t_{50\%}$.

The interrupted stress relaxation tests were performed using a single strain rate 10 s^{-1} in the temperatures range 950–1250 °C and strain range 0.2–0.6 to have different deformation parameters for evaluating the microstructure evolutions during roughing.

To get the starting prior austenite grain size, the samples were heated at 10 °C/s to 1250 °C and held for 120 s for homogenization then quenched in water, see Fig. 2.

2.3. Microstructure analysis

With the aim of studying the microstructure, the simulated samples were cut from the middle, mounted, grinded and polished. To reveal the prior austenite grains, the polished samples were left for two days before etching. The etchant was prepared using 4 g picric acid, 4.5 g ammonium chloride (NH_4Cl), 1 g sodium sulfate (Na_2SO_4) and 1 ml wetting agent and completed to 100 ml using distilled water. The etchant was diluted to 50% using distilled water. Then the samples were etched in the diluted etchant at 60 °C for 60–75 s. Then the samples were repolishing using silica suspension (0.04 μm) to remove the substructure for 30–60 s under pressure of 5–10 N.

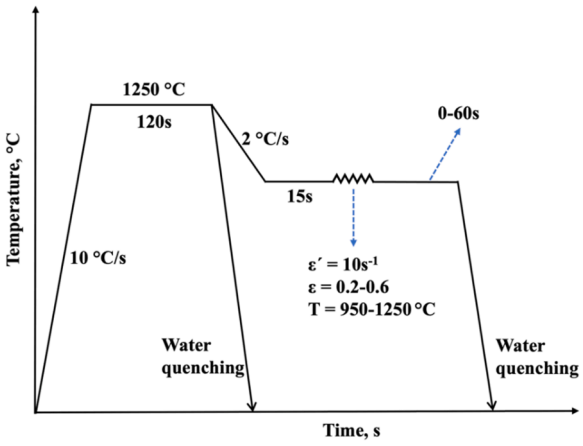

Fig. 2. Schematic diagram for stress-relaxation test on Gleeble thermo-mechanical simulator.

The prior austenite grain size and their size distributions were calculated semi-automatically from laser scanning confocal microscopy (LSCM) images by linear intercept method using a novel calculation tool developed by one of the authors and described in more details in [23]. In brief, firstly, a linear intercept interval data set is obtained using a self-made GUI tool, grain size calculator [23]. A novel fitting technique is then applied to fit a probability density function to the data set. The method is discussed in detail in [24], but the basic idea is that n^{th} order Taylor polynomials are applied in fitting to the cumulative probability density formed with the linear intercept interval data set, and the resulting equation is derivated to obtain the probability density function.

3. Results and discussion

3.1. Initial microstructure of steels

Fig. 3a and b show the prior austenite grains at the central area of the sample as well as the average PAGS of the investigated steels without deformation. The initial PAGS of 0Mo and 0.25Mo steels are measured to be 454 μm and 344 μm, respectively. These results are based on the analysis of a combined figure consisting of 4 micrographs of the presented in Fig. 3a and b. Both steels show a wide range of size distribution, see Fig. 3c and d. Compared to 0Mo steel, addition of Mo led to much lower frequency of very large grains due to the solute drag effect of Mo on the grain boundaries migrations which decrease the grain coarsening at high temperatures.

Table 1
Chemical composition of the investigated steels (in wt%), starting prior austenite grain size (PAGS), the calculated non-recrystallization (T_{nr}) and the dissolution temperatures of precipitates.

Steel Design	C	Si	Mn	Cr	Ni	Mo	Al	B	N	PAGS before deformation, μm	T_{nr} (°C)[a]	T (dissolution of BN) (°C)[b]	T (dissolution of AlN) (°C)[b]
0Mo	0.16	0.2	1.0	0.5	0.5	–	0.03	0.0015	0.0050	454	901	1124.07	1059.61
0.25Mo	0.16	0.2	1.1	0.5	0.5	0.25	0.03	0.0015	0.0043	344	913	1110.16	1044.89

[a] Calculated using $Tnr = 887 + 464C + \left(6445Nb - 644\sqrt{Nb}\right) + 500V + 363Al - 357Si + (400Mo - 175\sqrt{Mo})$ [2]

[b] Calculated using Thermo-Calc® 2022a with data base TCFE9

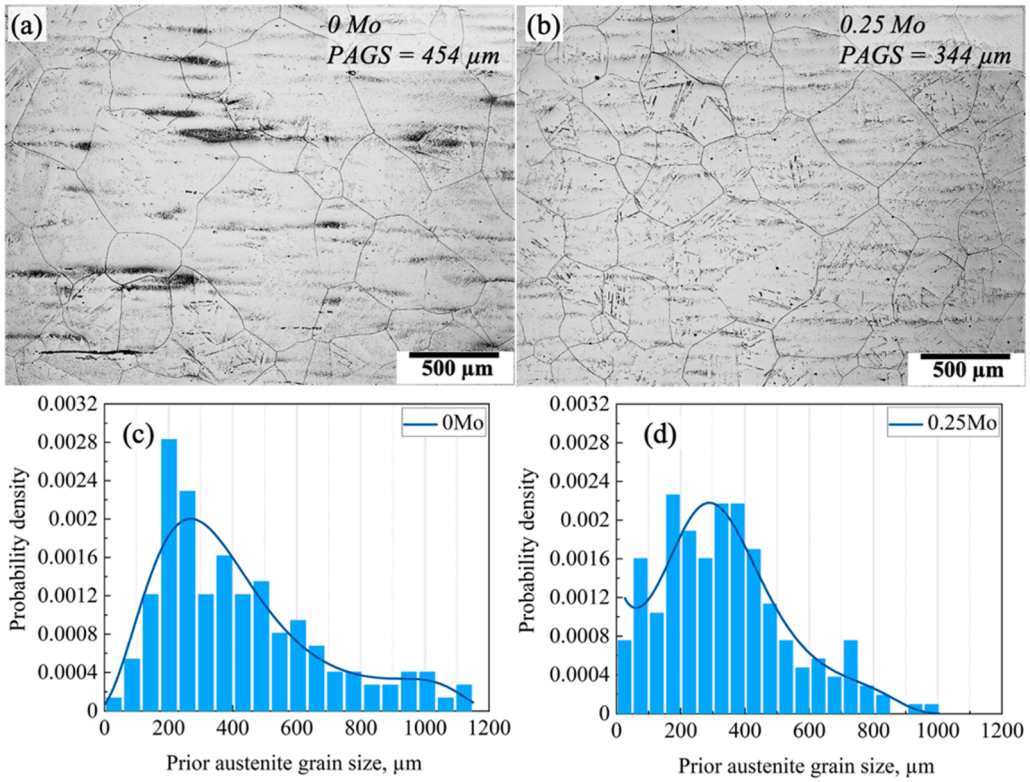

Fig. 3. LSCM micrographs of the studied steels after homogenization at 1250 °C and the corresponding probability density for (a, c) 0Mo and (b, d) 0.25Mo steels respectively.

3.2. Thermodynamic calculations

Thermodynamic calculations were performed using commercial Thermo-Calc software version 2022a and the database TCFE9. Fig. 4 shows the equilibrium precipitates formed in austenite in the temperature range 900–1300 °C for 0Mo and 0.25Mo steels. In case of 0Mo steel, AlN and BN are formed below 1059 °C and 1124 °C (the solubility temperatures given in Table 1) respectively and their volume fraction increased by decreased temperature, see Fig. 4. Similar precipitates were formed for 0.25Mo steel. However, BN and AlN were formed at a lower temperature, 1110 °C and 1044 °C respectively compared to 0Mo steel. Based on the thermodynamic calculations, the selected homogenization temperature, 1250 °C is suitable for complete dissolution of all precipitates and provides only austenite as starting phase.

3.3. Flow stress and relaxation behavior

Typical true stress-true strain curves for 0Mo and 0.25Mo steels reheated at 1250 °C for 120 s then compressed at 10 s^{-1} at temperatures ranging from 950° to 1250°C are shown in Fig. 5a. Fig. 5a show work hardening and dynamic recovery prior to stress relaxation at all deformation temperature. Thus, the static restoration (recovery and recrystallization) process can be characterized using the relaxation after hot compression [2]. The flow stress of the examined steels is, as predicted, highly influenced by the deformation temperature. For both steels, the flow stress decreases as the deformation temperature increases. This is due to a decrease in work hardening because of decreased dislocation motion resistance [25]. Compared to 0Mo steel, the addition of Mo increases the flow stress throughout all deformation temperatures. This is

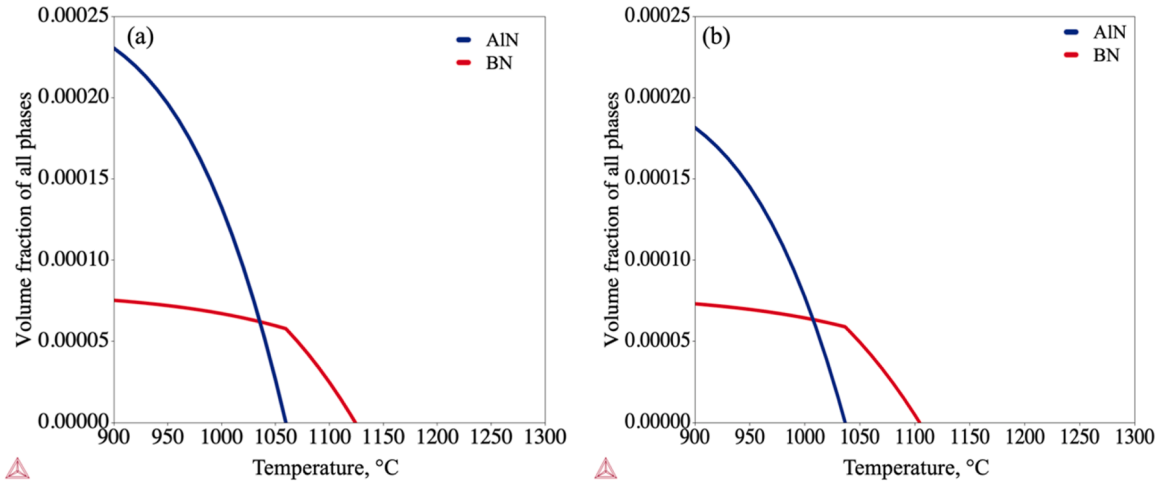

Fig. 4. Thermodynamic calculations for precipitate types formed in the investigated steels (a) 0Mo (b) 0.25Mo at high temperature.

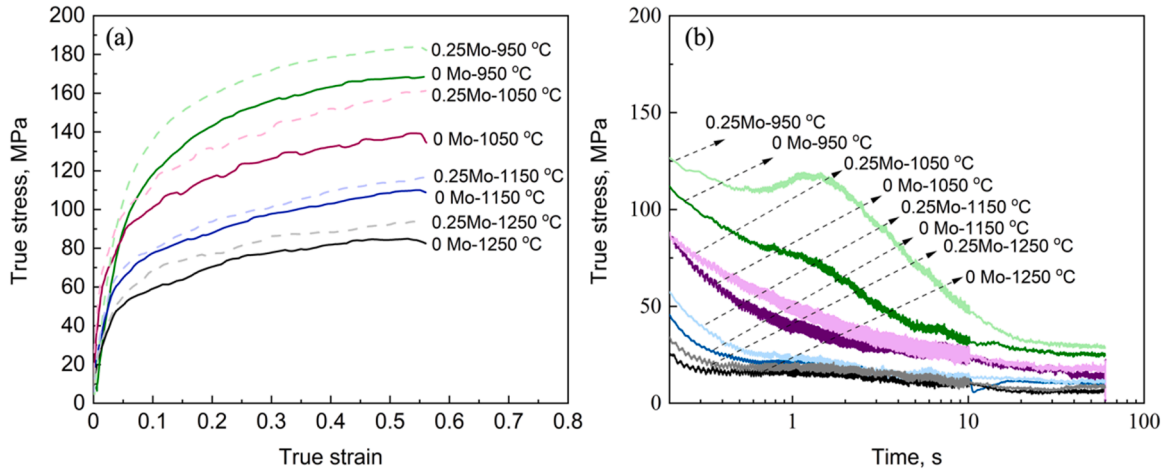

Fig. 5. Typical true stress-true strain curves (a) and typical stress-relaxation curves (b) for 0Mo and 0.25Mo steels. The samples reheated at 1250 °C then hot-compressed to 0.6 strain with strain rate 10 s^{-1} at the temperature range 950–1250 °C and recorded for 60 s after compression.

mainly due to the solid solution strengthening caused by Mo addition [26].

Fig. 5b shows typical stress-relaxation curves (true stress vs. log-relaxation time) for 0Mo and 0.25Mo steels compressed at 10 s^{-1} at temperatures ranging from 950° to 1250°C, which display three stages on the logarithmic time scale. The early and end linear stages on the curves correspond to the occurrence of static recovery (SRV), whereas the intermediate fast fall in the stress level indicates the SRX or MDRX process [14,27].

Avrami exponents for 0.25Mo steel are in the ranges of 1.20 – 1.44, 1.49 – 1.81 and 1.05 – 1.75 at strains 0.2, 0.4 and 0.6 respectively. While the Avrami exponents for 0Mo steel are in the ranges of 1.16 – 1.37, 1.31– 1.57 and 1.23 – 1.90 at strains 0.2, 0.4 and 0.6 respectively. Avrami exponent is roughly between 1.05 and 1.90 for both steels which agreed with the range obtained by Perttula et al. [28] for different steel grades and within the reported values (0.34–2) in other studies [28–32]. Moreover, it shows a little dependency on the temperature as it decreases with increasing the temperature which agreed with the results reported by *Facusseh* et al. [18].

Table 2 gives some values of Zurob fitting parameters including the activation enthalpy U_a, activation volume of recovery V_a and the activation energy for the diffusion of alloying elements Q_d for the investigated steels. The obtained values also have physical meaning, so they can be used to estimate the quality of the fitted results and are comparable with results reported by other authors [20]. It must be noted that the values can have some error due to the nature of the relaxation test, which often has some noise, as well as the numerical fitting method, where multiple variables are simultaneously fitted.

A comparison is made to the obtained fitting parameters values from 0Mo steels, addition of Mo increases U_a, V_a, and Q_d at all deformation temperatures and applied strains. There is a clear effect of temperature and the applied strain on the U_a, V_a, and Q_d. The values of U_a decreased slightly by about 1.58% and 3.06% for 0Mo and 0.25Mo steels when the temperature increased from 950 °C to 1150 °C at the lowest applied strain, respectively. At high applied strain i.e., 0.4 and 0.6, U_a decreased when the temperature increased from 950 °C to 1150 °C by about 13–16% and 24–25% for 0Mo and 0.25Mo steels, respectively. The values of V_a are decreased significantly at all applied strains for both investigated steels when the temperature increased from 950 °C to 1150 °C as illustrated in Table 2. The values of Q_d decreased slightly at the lowest strain when the temperature increased from 950 °C to 1150 °C by about 5% and 2% for 0Mo and 0.25Mo steels, respectively. At high applied strain i.e., 0.4 and 0.6, Q_d decreased when the temperature increased from 950 °C to 1150 °C by about 9–13% and 9–10% for 0Mo and 0.25Mo steels, respectively. The value of surface to volume ratio fitting parameter (S_v) is set as constant value of 80,839.75 m^{-1}. So, the product of geometrical factor fitting parameter (K) x surface to volume ratio fitting parameter (S_v), resulting in a comparable result with those obtained by *Pohjonen* et al.[20].

Fig. 6 shows the difference (in %) for fitting variables U_a, V_a and Q_d between deformation temperatures 950 and 1150 °C with strains 0.2–0.6 for both investigated steel grades. Increasing temperature decreases the parameter value in all cases, but the values vary greatly. For higher strains, the decrease seems to be more significant. These results are in line with common recrystallization theory, showing that recrystallization occurs more easily with increasing temperature. The results also show some variance, which is to be expected due to reasons mentioned earlier, as well as the test series having relatively few datapoints per test parameter.

Table 2
Some values of the parameters obtained from Zurob fitting model for different deformation parameters.

Steel	Temperature (°C)	Strain	U_a (J/mol)	Change (%)	V_a (m^3)	Change (%)	Q_d (J/mol)	Change (%)	KS_v (1/m)
0Mo	950	0.2	2.91×10^5	-1.58	9.04×10^{-28}	-75.65	8.73×10^4	-4.88	965
	1150	0.2	2.87×10^5		2.20×10^{-28}		8.30×10^4		5657
	950	0.4	2.76×10^5	-16.06	2.84×10^{-28}	-99.22	8.87×10^4	-8.49	4026
	1150	0.4	2.32×10^5		2.21×10^{-30}		8.11×10^4		5507
	950	0.6	2.81×10^5	-12.68	4.03×10^{-28}	-98.09	8.83×10^4	-13.39	3642
	1150	0.6	2.45×10^5		7.72×10^{-30}		7.64×10^4		2780
0.25Mo	950	0.2	3.11×10^5	-3.06	9.23×10^{-28}	-51.73	9.45×10^4	-2.19	2966
	1150	0.2	3.02×10^5		4.46×10^{-28}		9.24×10^4		4240
	950	0.4	3.16×10^5	-23.67	8.15×10^{-28}	-99.41	1.01×10^5	-8.53	4480
	1150	0.4	2.41×10^5		4.84×10^{-30}		9.22×10^4		9836
	950	0.6	3.08×10^5	-24.85	4.59×10^{-28}	-99.41	1.03×10^5	-9.88	1660
	1150	0.6	2.32×10^5		2.71×10^{-30}		9.31×10^4		7386

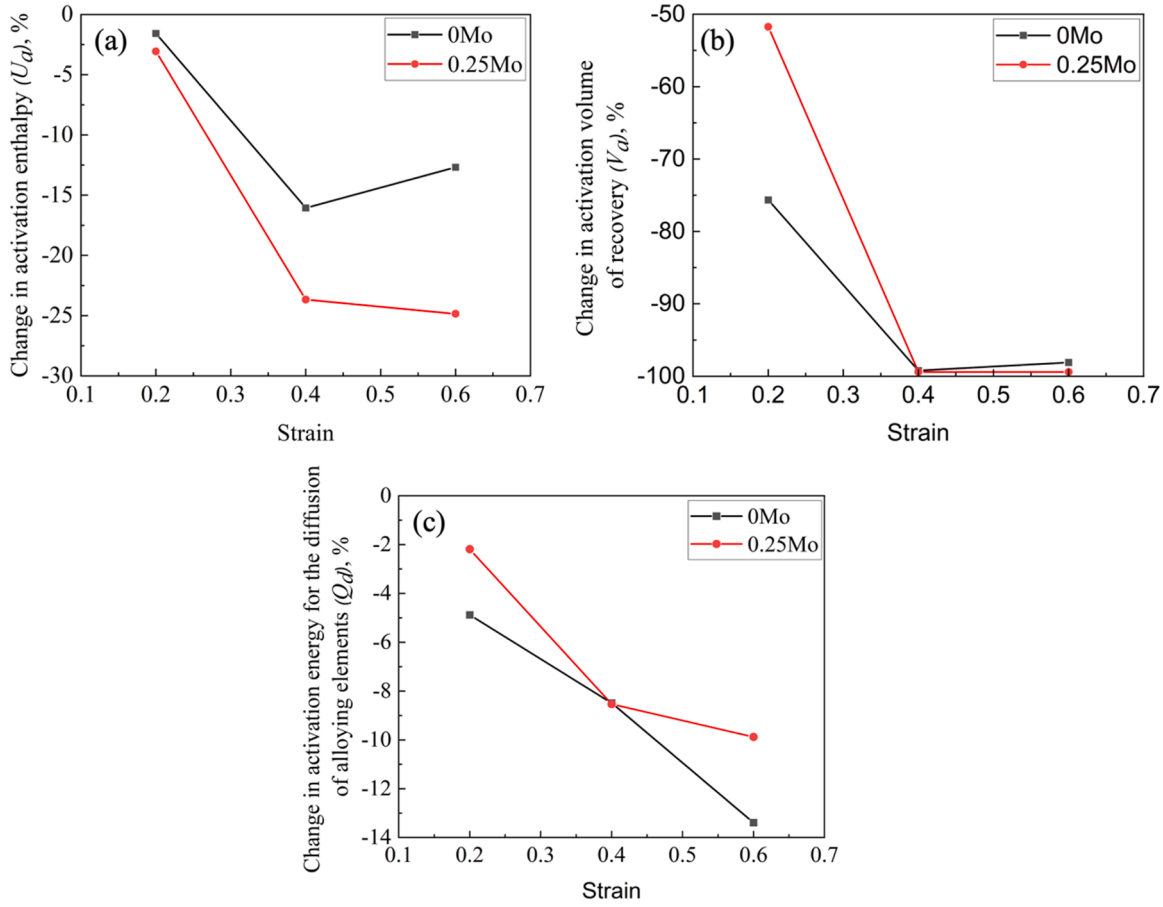

Fig. 6. Change (%) in the activation enthalpy U_a, activation volume of recovery V_a and the activation energy for the diffusion of alloying elements Q_d for the investigated steels due to temperature increase from 950° to 1150°C.

3.4. Effect of the deformation parameters on SRX kinetics and microstructure

3.4.1. Effect of deformation temperature

The kinetics of SRX process as a function of deformation parameters were determined using the analysis results of stress relaxation curves. The recrystallized fraction vs. time curves computed from the stress relaxation curves were used to calculate the $t_{50\%}$. In every case, complete softening was accomplished.

Fig. 7 show examples of recrystallized fraction versus time curves fitted with Zurob type-curves of 0Mo and 0.25Mo steels compressed to a true strain of 0.6 with strain rate 10 s^{-1} in the temperature range 950–1250 °C. Fig. 7 illustrates the accelerating effect of increasing the deformation temperature on the kinetics of SRX. The increased deformation temperature intensifies atoms' thermal vibrations, leading in high energy and instability at grain boundaries, contributing to the onset of SRX [33]. For instance, in the case of 0Mo steel, $t_{50\%}$ decreased from 4.09 s at 950 °C to 0.05 s at 1250 °C (see Fig. 7a). In the case of 0.25Mo

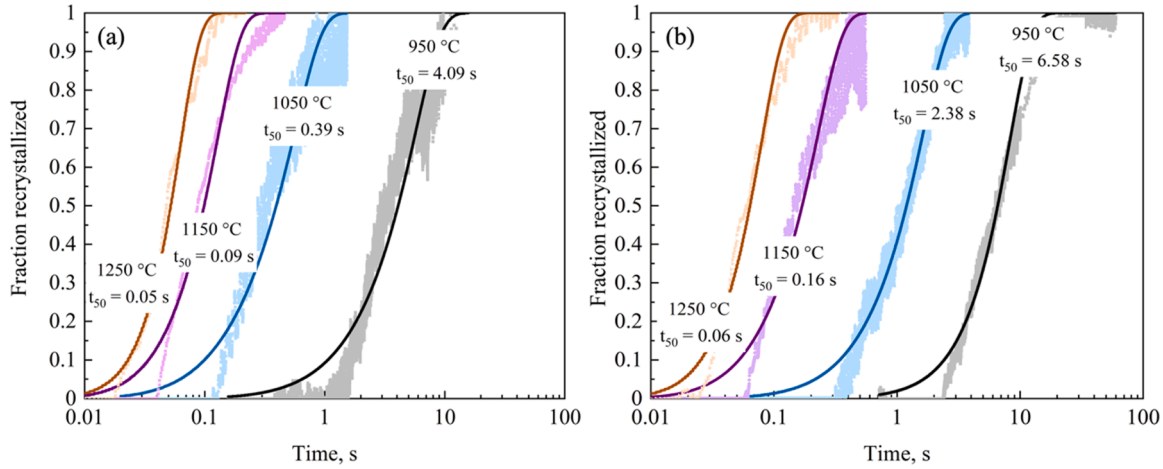

Fig. 7. Recrystallized fraction vs. time data calculated from stress relaxation curves and fitted with Zurob-type curves for (a) 0Mo steel and (b) 0.25Mo steel after hot-compression to 0.6 strain at 10 s^{-1} at temperature range 950–1250 °C.

steel, $t_{50\%}$ decreased from 6.58 s at 950 °C to 0.06 s at 1250 °C (see Fig. 7b). Addition of Mo decreases the rate of SRX, for example at 1050 °C, $t_{50\%}$ increased from 0.39 s to 2.38 s

Fig. 8 shows the microstructure evolution and the probability density of prior austenite grains for 0Mo and 0.25Mo steels after deformation with true strain 0.6 and strain rate 10 s^{-1} at temperature range 1050–1250 °C and with zero holding time. The peakshapes of grain size distribution vary dramatically when deformation temperature rises. It show that the average PAGS increased with increasing deformation temperature as a result of grain growth and the number of small grains decreased which is clearly visible from the microstructure and probability density of PAGS. This is mostly owing to the fact that the larger

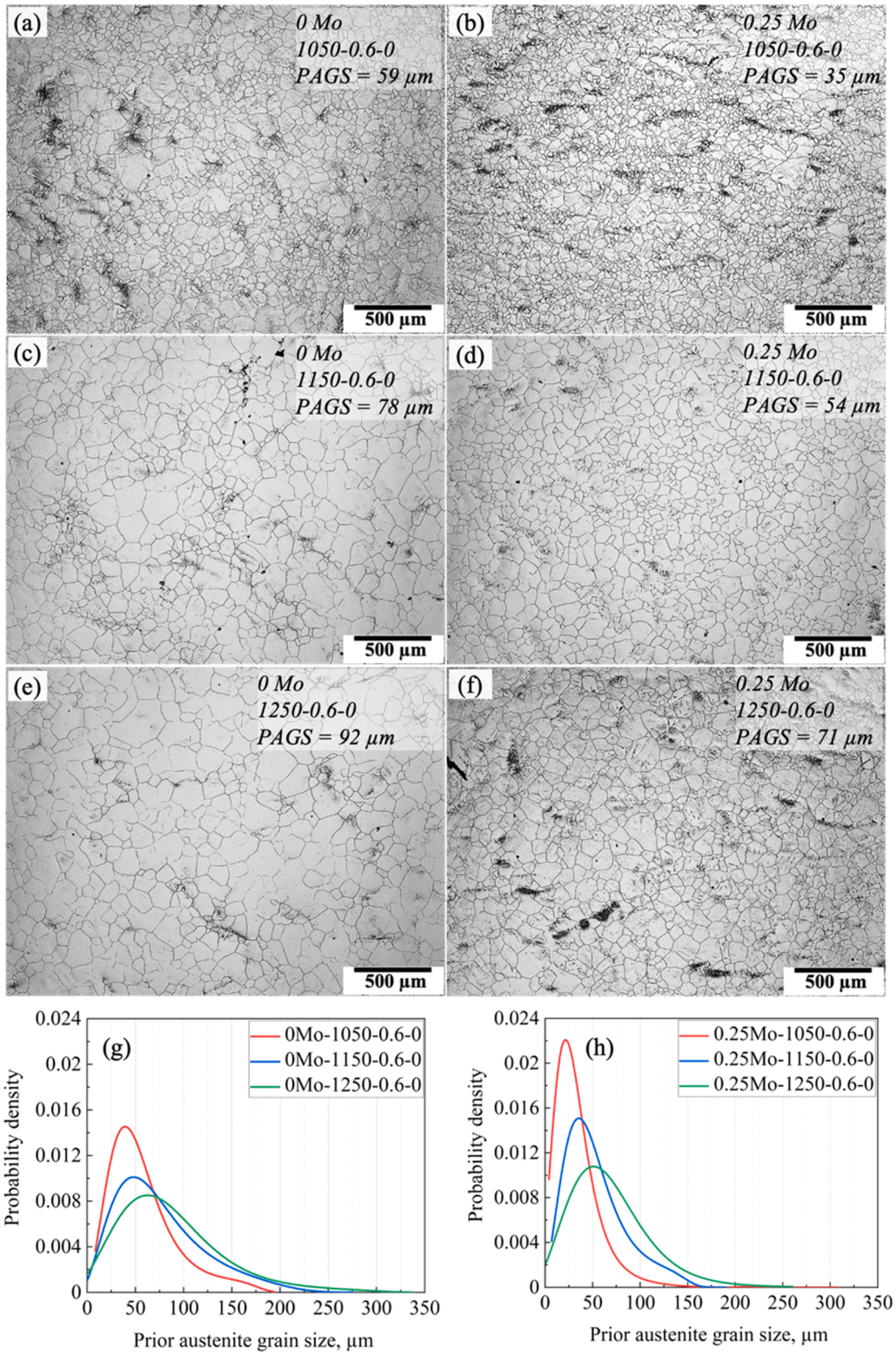

Fig. 8. LSCM micrographs of the studied steels after hot-compression to true strain 0.6 with strain rate 10 s^{-1} at temperature range 1050–1250 °C and the corresponding probability density (a, c, e, g) and (b, d, f, h) for 0Mo and 0.25Mo steels respectively.

deformation-stored energy at higher temperatures increases SRX due to the higher atomic activities, high nucleation rate and grain boundary migration velocity [3,34,35].

Compared to 0Mo steel, 0.25Mo steel has higher probability density of small grains at all deformation temperatures, see Fig. 8g and h. This illustrates the high number of nucleations and slower rate of grain growth due to the solute drag effect caused by the Mo addition.

3.4.2. Effect of applied strain

Fig. 9 shows examples of recrystallized fraction versus time curves fitted with Zurob type-curves of 0Mo and 0.25Mo steels compressed with true strains 0.2, 0.4 and 0.6 with strain rate 10 s^{-1} at 1150 °C. Fig. 9 illustrates the accelerating effect of increasing the applied true strain on the kinetics of SRX. For instance, in the case of 0Mo steel, $t_{50\%}$ decreased from 1.59 s after applying 0.2 true strain to 0.1 s after applying 0.6 true strain (see Fig. 9a). In the case of 0.25Mo steel, $t_{50\%}$ decreased from 1.77 s after applying 0.2 true strain to 0.16 s after applying 0.6 true strain. Increasing the applied strain has a significant effect on accelerating the SRX process because of the multiplication of dislocation density leading to an increase in the stored energy and thereby the driving force for SRX which accelerate the recrystallization [34,36,37].

Fig. 10 shows the microstructure evolution and the probability density of prior austenite grain for 0Mo and 0.25Mo steels after deformation to true strains 0.2, 0.4 and 0.6 with strain rate 10 s^{-1} at 1150 °C and with zero holding time. Higher strain produces more tiny grains at 0 s. The little grains are most likely newly nucleated recrystallized grains, and their growing abundance indicates that higher strains begin recrystallization faster. Higher strain causes additional dislocation cells or tangles to form on the grain boundaries, increasing the driving force for recrystallization. It is significant in the case of 0.25Mo steel compared to 0Mo steels which clearly visible from the probability density of PAGS, see Fig. 10g and h. Thereby, the average PAGS decreased in both steels with increasing the applied strain.

3.4.3. Effect of holding time

Fig. 11 shows the prior austenite grains as well as their probability density for 0Mo and 0.25Mo steels after deformation to true strain 0.2 with strain rate 10 s^{-1} at 1050 °C and with three holding times 0, 30 and 60 s. Holding time has a significant influence on grain size, as illustrated in Fig. 11. Many tiny grains are present at 0 s in both steels, because of the fresh nucleating grains. However, the nucleation starts very fast in case of 0Mo steel compared to 0.25Mo steel. In case of 0Mo steel, small grains cover almost all the test piece while in the case of 0.25Mo, prior grain boundaries become serrated, and a few ultrafine equiaxed recrystallized grains develop at the original grain boundaries. Thereby, the average PAGS of 0Mo is smaller than that of 0.25Mo steel. For 30 and 60 s holding time, the average PAGS increases with increasing holding time. This is likely since recrystallization has completed, and the test sample has progressed to the grain growth stage, where new nucleated grains continue growing. Because SRX is a thermal activation process connected to atomic diffusion, extending the holding time provides more time for atomic diffusion, increasing the SRX [34,37,38]. Moreover, the dislocation density decreased with increasing the holding time [3]. The growth rate in case of 0.25Mo steel is much slower compared to the 0Mo steel subsequently, there is not much difference in the probability density as well as the average PAGS of 0.25Mo steel at 30 s and 60 s compared to 0Mo steel, see Fig. 11g and h.

3.5. Apparent activation energy of recrystallization (Q_{app}) and activation energy of SRX (Q_{rex})

The dependence of SRX kinetics of 0Mo and 0.25Mo steels on temperature are illustrated in Fig. 12. Based on $t_{50\%}$ readings for the specimens deformed to 0.6 strain at strain rate 10 s^{-1} in temperature range 950–1250 °C, the apparent activation energy (Q_{app}) of recrystallization was calculated as 206 and 212 kJ/mol for 0Mo and 0.25Mo steels respectively, see Fig. 12. These values fall in the range of Q_{app} (177–283 kJ/mol) reported in literature for other steels [39]. The activation energy of SRX (Q_{rex}) depend on Q_{app}, the power of strain rate q and the deformation activation energy (Q_{def}). Q_{rex} can be calculated using Eq. (5). A high Q_{rex} value indicates that more energy or time is required to initiate the recrystallization process.

$$Q_{rex} = Q_{app} - q * \quad Q_{def} \tag{5}$$

For developing the regression model for the Q_{rex} of hot deformed austenite, Somani et al. [21,40,41] assumed the Q_{def} of 340 kJ/mol for C-Mn steels. So by assuming the Q_{def} is 340 kJ/mol and q is − 0.21 [2], Q_{rex} of 277 and 283 are obtained for 0Mo and 0.25Mo steels respectively. Q_{rex} (in J/mol) can be calculated for C–Mn and microalloyed steels using Eq. (6,7) which is based on linear regression analysis [6,41].

$$Q_{rex} = 3803CF + 109418 \tag{6}$$

Where CF is the composition factor given by.

$$\mathrm{CF} = 2\mathrm{Cr} + 10\mathrm{Cu} + 15\mathrm{Mn} + 50\mathrm{Mo} + 60\mathrm{Si} + 70\ \mathrm{V} + 230\mathrm{Ti} + 700\ \mathrm{Nb} \tag{7}$$

Where the elements are in wt%. The calculated values of Q_{rex} using Eqs. (3,4) are 216 and 269 kJ/mol for 0Mo and 0.25Mo respectively which are lower than the experimentally obtained values (277 and

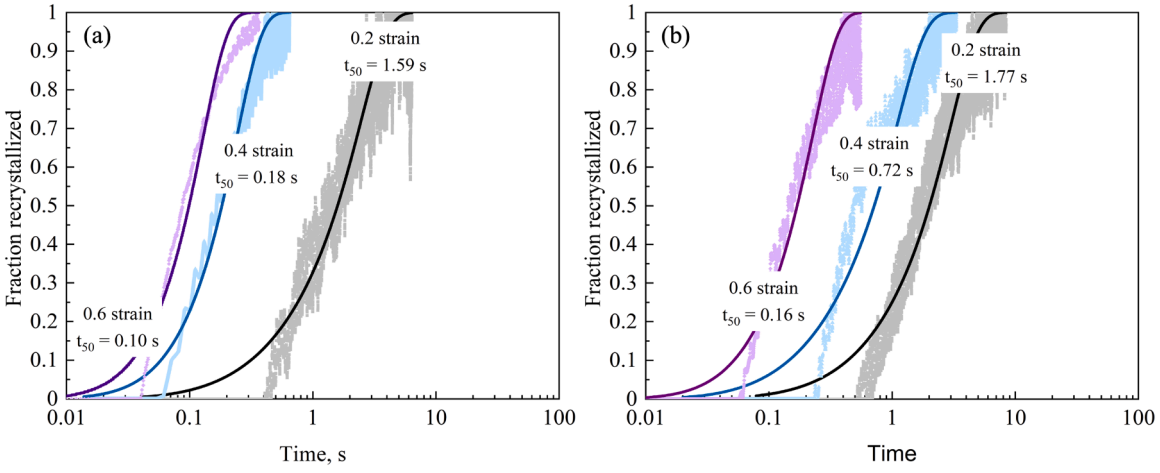

Fig. 9. Recrystallized fraction vs. time data calculated from stress relaxation curves and fitted with Zurob-type curves for (a) 0Mo steel and (b) 0.25Mo steel after hot-compression to 0.2, 0.4 and 0.6 strain at 10 s^{-1} at 1150 °C.

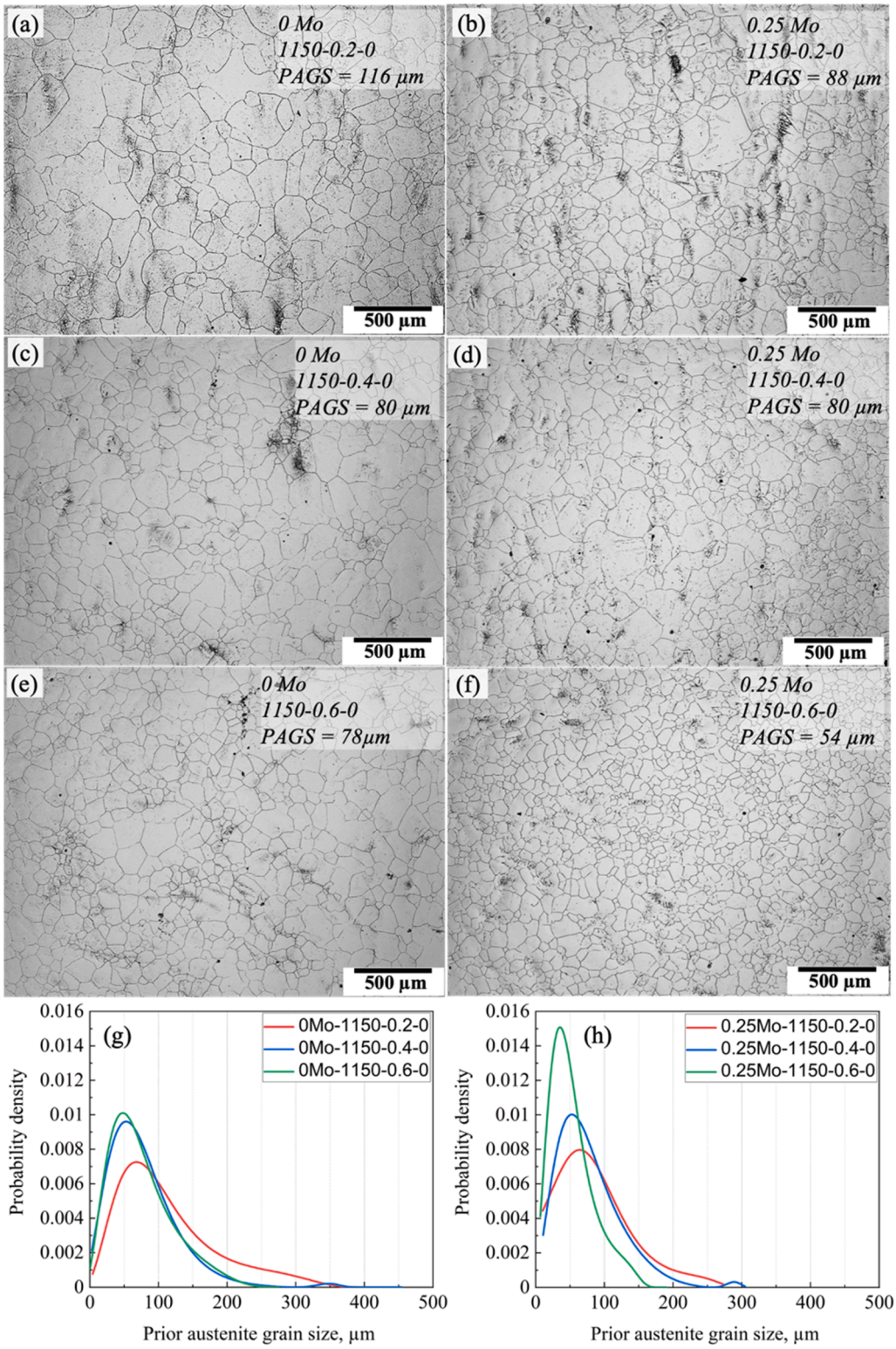

Fig. 10. LSCM micrographs of the studied steels after hot-compression at 1150 °C with strain rate 10 s^{-1} to true strain 0.2, 0.4 and 0.6 and the corresponding probability density (a, c, e, g) and (b, d, f, h) for 0Mo and 0.25Mo steels respectively.

283 kJ/mol). This illustrates that prediction of Q_{rex} using Eq. (6,7) is not accurate for the investigated steels.

3.6. Estimation of the power of strain (p)

The $t_{50\%}$ times for SRX show a strong dependency on the applied true strain, as $t_{50\%}$ times decrease when increasing the applied true strain. Increasing the applied strains led to increase in the dislocation density which provides the driving force for SRX [1]. Based on the plotted results in Fig. 13, the strain exponent (p) was estimated from the slope of the line fits of the data points in the log-log plot to be about − 1.90 and − 2.57 in the strain range of 0.2–0.6 and 0.3–0.5 for 0Mo and 0.25Mo

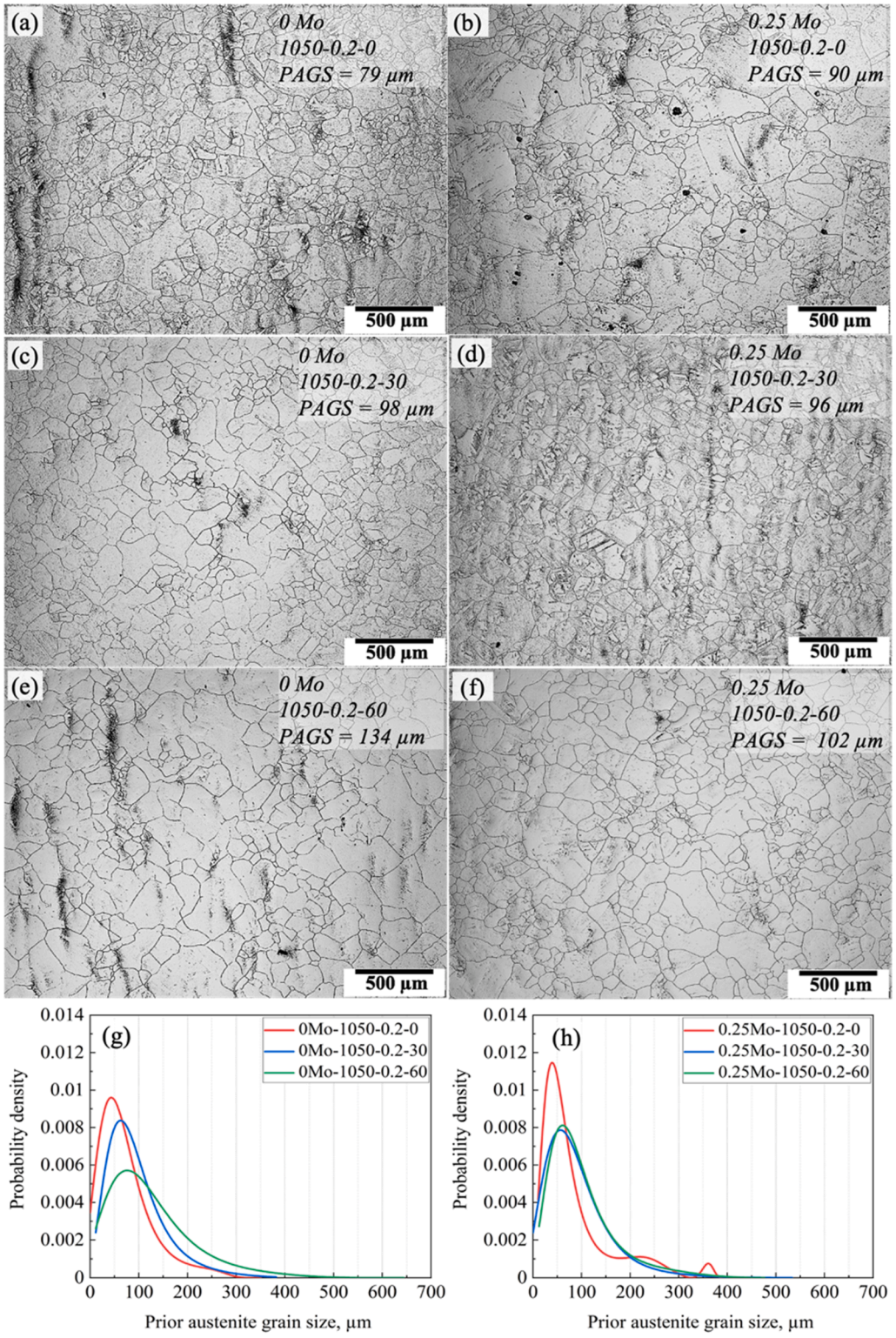

Fig. 11. LSCM micrographs of the studied steels after hot-compressed at 1050 °C with strain rate 10 s^{-1} to true strain 0.2 with different holding times 0, 30 and 60 s and the corresponding probability density (a, c, e, g) and (b, d, f, h) for 0Mo and 0.25Mo steels respectively.

steels, respectively. The strain exponent has a broad range of values recorded in literature, see [13,14,42]. The current values are close to the values of p (−2 and −2.6) reported in literature [43–45]. Also, the current values of p are comparable with those values reported for C-Mn steels and medium carbon spring steels (−2.5) and Nb/Nb-Ti steels (−2.8) which are based on stress relaxation tests [27]. The strain exponent of − 2.5 was also used by Hodgson and Gibbs [46] for C-Mn, Ti-, and V-steels. Moreover, the values of p in the current study are comparable with those reported by Kaikkonen et al. [2] for microalloyed medium carbon bainitic steels which range from − 1.7 to − 2.7.

3.7. Fractional softening equations for SRX

The power of strain rate q − 0.23 was derived from a prior regression

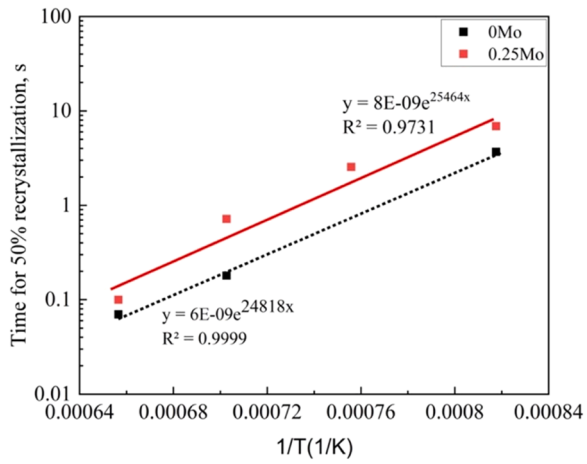

Fig. 12. Estimation of Q_{app} of the investigated steels.

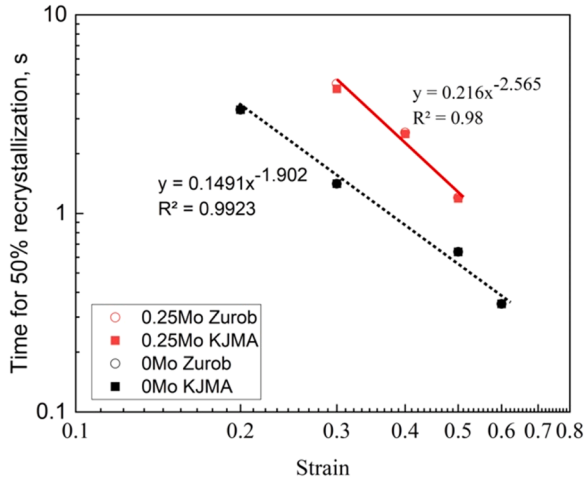

Fig. 13. Dependence of $t_{50\%}$ on strain for the investigated steels deformed at 1050 °C. The plotted data including $t_{50\%}$ calculated after applying KJMA and Zurob-type fitting.

model that could predict the static recrystallization of various carbon and microalloyed steels [47]. All the reported values of q in literature fall within a small range − 0.11 to − 0.23 which indicates the weak dependency of SRX on the strain rate, irrespective of chemical composition [39]. Combining the above values for Q_{app}, p, and q in Eq. (1) with the power of grain size described by the relation $s = 2.13d - 0.105$ [39], the constant A for the two steels is obtained. Therefore, the SRX rate can be described using the following SRX equations:

$$0\text{Mo steel}: \quad t_{50\%} = 4.43 \bullet \quad 10^{-12} \quad \varepsilon^{-1.9}\dot{\varepsilon}^{-0.23} d^{s} \exp\left(\frac{206000}{RT}\right) \tag{9}$$

$$0.25\text{Mo}: \text{steel}: \quad t_{50\%} = 2.29 \bullet \quad 10^{-12} \quad \varepsilon^{-2.57}\dot{\varepsilon}^{-0.23} d^{s} \exp\left(\frac{212000}{RT}\right) \tag{10}$$

3.8. Comparison between the experimental and predicted results

A comparison between the predicted values of $t_{50\%}$ times using equations (9,10) and with those obtained experimentally for the current investigated steels are illustrated in Fig. 14 which shows a good agreement although results are somewhat scattered. This suggests that the developed kinetic equations could provide a good estimation of SRX behavior for metal-forming processes.

4. Conclusions

To create suitable thermomechanically controlled rolling procedures that avoid partial recrystallization and produce fine grain during roughing, the static recrystallization characteristics and grain growth during roughing were evaluated using the interrupted stress relaxation test on Gleeble 3800 thermomechanical simulator over a wide range of temperatures (950–1250 °C) and strains (0.2–0.6) for newly-developed low-carbon CrNiMnB ultrahigh-strength steel with and without molybdenum addition. The effect of Mo on the static recrystallization kinetics was investigated. A novel semi-automatic stress relaxation test reading tool with a graphical user interface was created to automate as many steps as possible which work smoothly and successfully for all results reported in the current study. Moreover, it overcomes the difficulties in determination of the onset of static recrystallization manually from the stress relaxation curves especially at high temperatures. The conclusions can be drawn as follows:

1. During compression under all deformation parameters, strain hardening, and dynamic recovery occurred. The flow stress in case of 0.25Mo steel are higher than those of 0Mo steel.
2. The static recrystallization kinetics were successfully revealed under various conditions using the interrupted stress relaxation method and new static recrystallization equations were established using the recorded stress relaxation data for explaining static recrystallization in hot-deformed austenite of 0Mo and

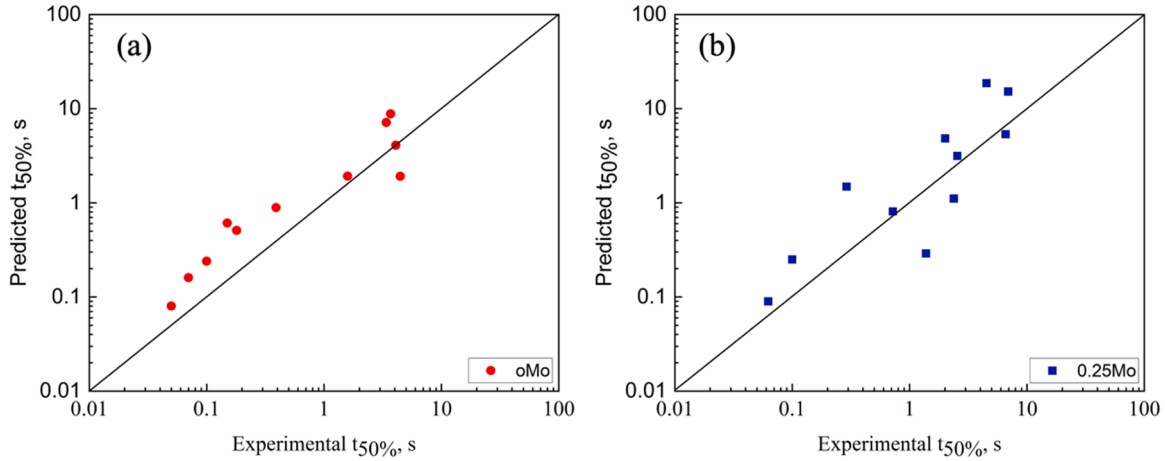

Fig. 14. Prediction vs. experimental $t_{50\%}$ times: (a) 0Mo steel and (b) 0.25Mo steel.

0.25Mo steels. Addition of Mo retard the SRX kinetics. The equations expressed as:

$$0\text{Mo steel}: \quad t_{50\%} = 4.43 \bullet \quad 10^{-12} \quad \varepsilon^{-1.9}\dot{\varepsilon}^{-0.23}d^{s}\exp\left(\frac{206000}{RT}\right)$$

$$0.25\text{Mo steel}: \quad t_{50\%} = 2.29 \bullet \quad 10^{-12} \quad \varepsilon^{-2.57}\dot{\varepsilon}^{-0.23}d^{s}\exp\left(\frac{212000}{RT}\right)$$

3. The materials correlation constant (Avrami exponent, n) is roughly between 1.05 and 1.90 for both 0Mo and 0.25Mo steels.
4. The values of Zurob fitting parameters including the activation enthalpy U_a, activation volume of recovery V_a and the activation energy for the diffusion of alloying elements Q_d increases with the addition of Mo at all deformation temperatures and applied strains. Increasing temperature decreases the parameter value in all cases, but the values vary greatly. For higher strains, the decrease seems to be more significant.
5. The activation energy of static recrystallization (Q_{rex}) of 277 and 283 kJ/mol are obtained for 0Mo and 0.25Mo steels respectively.
6. The SRX and grain growth are highly sensitive to the deformation temperature, applied strain and holding time.
7. A comparison was performed between the experimental and the predicted values using the developed SRX kinetic equations, showing a good agreement.
8. The peakshapes of grain size distribution vary dramatically when deformation temperature rises, indicating that deformation temperature has a major impact on SRX. It shows that the average PAGS increased with increasing deformation temperature as a result of grain growth and a decrease in the number of small grains.
9. Higher strain produces more newly nucleated recrystallized grains and their growing abundance indicates that higher strains accelerate recrystallization rate.
10. Holding time has a significant influence on grain size distribution and average PAGS of 0Mo steel compared to 0.25Mo steel.

CRediT authorship contribution statement

Mohammed Ali: Funding acquisition, Conceptualization, Methodology, Formal analysis, Investigation, Writing – original draft, Writing – review & editing. **Oskari Seppälä**: Methodology, Formal analysis, Software, Writing – review & editing. **Timo Fabritius**: Project administration, Funding acquisition. **Jukka Kömi**: Funding acquisition.

Declaration of Competing Interest

The authors declare that they have no known competing financial interests or personal relationships that could have appeared to influence the work reported in this paper.

Data availability

The data that has been used is confidential.

Acknowledgment

The authors would like to thank Finnish Foundation for Technology Promotion for their financial support during this work through the program of postdoc in company (PoDoCo). Also, part of this work was conducted within the framework of the AMET project funded by Business Finland. Oskari Seppälä would like to acknowledge financial assistance of Business Finland, project FOSSA- Fossil-Free Steel Applications.

Appendix A. Supporting information

Supplementary data associated with this article can be found in the online version at doi:10.1016/j.mtcomm.2022.104676.

References

[1] P.D. Hodgson, S.H. Zahiri, J.J. Whale, The static and metadynamic recrystallization behaviour of an X60 Nb microalloyed steel, ISIJ Int. 44 (2004) 1224–1229, https://doi.org/10.2355/isijinternational.44.1224.
[2] P.M. Kaikkonen, M.C. Somani, L.P. Karjalainen, J.I. Kömi, Flow stress behaviour and static recrystallization characteristics of hot deformed austenite in microalloyed medium-carbon bainitic steels, Metals 11 (2021) 138, https://doi.org/10.3390/met11010138.
[3] L. Wang, S. Xiao, Z. Tang, P. Qian, C.W. Siyasiya, Study of static recrystallization behavior of austenite in a Ti–V microalloyed steel, Mater. Express 10 (2020) 1047–1056, https://doi.org/10.1166/mex.2020.1737.
[4] C.L. Miao, C.J. Shang, H.S. Zurob, G.D. Zhang, S.V. Subramanian, Recrystallization, precipitation behaviors, and refinement of austenite grains in high Mn, high Nb steel, Metall. Mater. Trans. A 43 (2012) 665–676, https://doi.org/10.1007/s11661-011-0895-5.
[5] C.M. Sellars, J.A. Whiteman, Recrystallization and grain growth in hot rolling, Met. Sci. 13 (1979) 187–194, https://doi.org/10.1179/msc.1979.13.3-4.187.
[6] M.C. Somani, L.P. Karjalainen, Validation of the new regression model for the static recrystallisation of hot-deformed austenite in special steels, Mater. Sci. Forum 467–470 (2004) 335–340, https://doi.org/10.4028/www.scientific.net/MSF.467-470.335.
[7] S.F. Medina, J.E. Mancilla, Influence of alloying elements in solution on static recrystallization kinetics of hot deformed steels, ISIJ Int. 36 (1996) 1063–1069, https://doi.org/10.2355/isijinternational.36.1063.
[8] S.F. Medina, A. Quispe, Improved model for static recrystallization kinetics of hot deformed austenite in low alloy and Nb/V microalloyed steels, ISIJ Int. 41 (2001) 774–781, https://doi.org/10.2355/isijinternational.41.774.
[9] M.R.G. Ferdowsi, D. Nakhaie, P.H. Benhangi, G.R. Ebrahimi, Modeling the high temperature flow behavior and dynamic recrystallization kinetics of a medium carbon microalloyed steel, J. Mater. Eng. Perform. 23 (2014) 1077–1087, https://doi.org/10.1007/s11665-013-0815-5.
[10] X.L. He, M. Djahazi, J.J. Jonas, J. Jackman, The non-equilibrium segregation of boron during the recrystalization of Nb-treated HSLA steels, Acta Metall. Mater. 39 (1991) 2295–2308, https://doi.org/10.1016/0956-7151(91)90012-P.
[11] P.P. Suikkanen, V.T.E. Lang, M.C. Somani, D.A. Porter, L.P. Karjalainen, Effect of silicon and aluminium on austenite static recrystallization kinetics in high-strength TRIP-aided steels, ISIJ Int. 52 (2012) 471–476, https://doi.org/10.2355/isijinternational.52.471.
[12] B. Pereda, B. López, J.M. Rodriguez-Ibabe, Role of Mo on static recrystallization kinetics in coarse grained Nb microalloyed steels, Mater. Sci. Forum 753 (2013) 453–458, https://doi.org/10.4028/www.scientific.net/MSF.753.453.
[13] J. Perttula, Physical Simulation of Hot Working (Doctoral thesis), University of Oulu, 1998.
[14] L.P. Karjalainen, J. Perttula, Characteristics of static and metadynamic recrystallization and strain accumulation in hot-deformed austenite as revealed by the stress relaxation method, ISIJ Int. 36 (1996) 729–736, https://doi.org/10.2355/isijinternational.36.729.
[15] M. Avrami, Kinetics of phase change. II Transformation-time relations for random distribution nuclei, J. Chem. Phys. 8 (1940) 212–224, https://doi.org/10.1063/1.1750631.
[16] Recrystallization and Related Annealing Phenomena, Elsevier, 2004. https://doi.org/10.1016/B978–0-08–044164-1. X5000–2.
[17] J. Majta, J.G. Lenard, M. Pietrzyk, Modelling the evolution of the microstructure of a Nb steel, ISIJ Int. 36 (1996) 1094–1102, https://doi.org/10.2355/isijinternational.36.1094.
[18] C. Facusseh, A. Salinas, A. Flores, G. Altamirano, Study of static recrystallization kinetics and the evolution of austenite grain size by dynamic recrystallization refinement of an eutectoid steel, Metals 9 (2019) 1289, https://doi.org/10.3390/met9121289.
[19] H.S. Zurob, C.R. Hutchinson, Y. Brechet, G. Purdy, Modeling recrystallization of microalloyed austenite: effect of coupling recovery, precipitation and recrystallization, Acta Mater. 50 (2002) 3077–3094, https://doi.org/10.1016/S1359-6454(02)00097-6.
[20] A. Pohjonen, O. Seppälä, A. Jokiranta, A. Kaijalainen, M. Somani, D. Porter, J. Larkiola, J. Kömi, Determination of static recrystallization and recovery parameters for steel by fitting model to stress relaxation data, J. Phys. Conf. Ser. 1270 (2019) 012013. https://doi.org/10.1088/1742–6596/1270/1/012013.
[21] M.C. Somani, D.A. Porter, L.P. Karjalainen, P.K. Kantanen, J.I. Kömi, D.K. Misra, Static recrystallization characteristics and kinetics of high-silicon steels for direct quenching and partitioning, Int. J. Mater. Res. 110 (2019) 183–193, https://doi.org/10.3139/146.111744.
[22] O. Seppälä, GUI tool to read stress relaxation test results (2022). ⟨https://github.com/osseppal/relax_reader⟩.
[23] S. Koskenniska, O. Seppälä, J. Kömi, A study on grain growth using a novel grain size calculation tool, Procedia Manuf. 50 (2020) 684–688, https://doi.org/10.1016/j.promfg.2020.08.123.

[24] O. Seppälä, A. Pohjonen, M. Ali, J. Larkiola, T. Fabritius, Analysis of grain size distribution evolution of steel during recrystallization and grain growth, in: Met. Form. 2022, Taiyuan, Shanxi, P.R. China, n.d.
[25] N. Yan, H.-S. Di, H.-Q. Huang, R.D.K. Misra, Y.-G. Deng, Hot deformation behavior and processing maps of a medium manganese TRIP steel, Acta Metall. Sin. Engl. Lett. 32 (2019) 1021–1031, https://doi.org/10.1007/s40195-018-0854-x.
[26] N. Singh, A.G. Kostryzhev, C.R. Killmore, E.V. Pereloma, Effect of Mo, Nb and V on hot deformation behaviour, microstructure and hardness of microalloyed steels, Mater. Sci. Forum 941 (2018) 3–8, https://doi.org/10.4028/www.scientific.net/MSF.941.3.
[27] M.C. Somani, L.P. Karjalainen, J.H. Bianchi, On the recrystallisation characteristics and kinetics of a 9SMn28 free cutting steel, Mater. Sci. Forum 558–559 (2007) 333–338, https://doi.org/10.4028/www.scientific.net/MSF.558-559.333.
[28] J.S. Perttula, L.P. Karjalainen, Recrystallisation rates in austenite measured by double compression and stress relaxation methods, Mater. Sci. Technol. 14 (1998) 626–630, https://doi.org/10.1179/mst.1998.14.7.626.
[29] A. Laasraoui, J.J. Jonas, Recrystallization of austenite after deformation at high temperatures and strain rates—analysis and modeling, Metall. Trans. A 22 (1991) 151–160, https://doi.org/10.1007/BF03350957.
[30] A.I. Fernández, B. López, J.M. Rodríguez-Ibabe, Relationship between the austenite recrystallized fraction and the softening measured from the interrupted torsion test technique, Scr. Mater. 40 (1999) 543–549, https://doi.org/10.1016/S1359-6462(98)00452-7.
[31] F. Arieta, C. Sellars, Activation volume and activation energy for deformation of Nb HSLA steels, Scr. Metall. Mater. 30 (1994) 707–712, https://doi.org/10.1016/0956-716X(94)90186-4.
[32] Y.G. Liu, J. Liu, M.Q. Li, H. Lin, The study on kinetics of static recrystallization in the two-stage isothermal compression of 300M steel, Comput. Mater. Sci. 84 (2014) 115–121, https://doi.org/10.1016/j.commatsci.2013.11.056.
[33] X. Sun, M. Zhang, Y. Wang, J. Liu, Microstructure evolution and kinetics of static recrystallization of medium Mn steel in the two-hit isothermal compression, Steel Res. Int. 92 (2021) 2000443, https://doi.org/10.1002/srin.202000443.
[34] F. Chen, D. Sui, Z. Cui, Static recrystallization of 30Cr2Ni4MoV ultra-super-critical rotor steel, J. Mater. Eng. Perform. 23 (2014) 3034–3041, https://doi.org/10.1007/s11665-014-1083-8.
[35] D. Dong, F. Chen, Z. Cui, Static recrystallization behavior of SA508-III steel during hot deformation, J. Iron Steel Res. Int. 23 (2016) 466–474, https://doi.org/10.1016/S1006-706X(16)30074-7.
[36] Z. Zeng, L. Chen, F. Zhu, X. Liu, Static recrystallization behavior of a martensitic heat-resistant stainless steel 403Nb, Acta Metall. Sin. (Engl. Lett.) 24 (2011) 381–389.
[37] H. Mao, R. Zhang, L. Hua, F. Yin, Study of static recrystallization behaviors of GCr15 steel under two-pass hot compression deformation, J. Mater. Eng. Perform. 24 (2015) 930–935, https://doi.org/10.1007/s11665-014-1264-5.
[38] Y.C. Lin, M.-S. Chen, J. Zhong, Study of static recrystallization kinetics in a low alloy steel, Comput. Mater. Sci. 44 (2008) 316–321, https://doi.org/10.1016/j.commatsci.2008.03.027.
[39] M.C. Somani, D.A. Porter, L.P. Karjalaien, P. Kantanen, J. Kömi, R.D.K. Misra, On the recrystallization characteristics and kinetics of two high-Si DQ&P steels, J. Phys. Conf. Ser. 1270 (2019), 012025, https://doi.org/10.1088/1742-6596/1270/1/012025.
[40] A.M. Elwazri, E. Essadiqi, S. Yue, Kinetics of metadynamic recrystallization in microalloyed hypereutectoid steels, ISIJ Int. 44 (2004) 744–752, https://doi.org/10.2355/isijinternational.44.744.
[41] M.C. Somani, L.P. Karjalainen, Modelling the deformation and annealing processes: physical and regression approaches, Mater. Sci. Forum 550 (2007) 583–588, https://doi.org/10.4028/www.scientific.net/MSF.550.583.
[42] C.M. Sellars, Modelling microstructural development during hot rolling, Mater. Sci. Technol. 6 (1990) 1072–1081, https://doi.org/10.1179/mst.1990.6.11.1072.
[43] A.M. Elwazri, E. Essadiqi, S. Yue, The kinetics of static recrystallization in microalloyed hypereutectoid steels, ISIJ Int. 44 (2004) 162–170, https://doi.org/10.2355/isijinternational.44.162.
[44] A.M. Elwazri, P. Wanjara, S. Yue, Metadynamic and static recrystallization of hypereutectoid steel, ISIJ Int. 43 (2003) 1080–1088, https://doi.org/10.2355/isijinternational.43.1080.
[45] S.F. Medina, V. Lopez, Static recrystallization in austenite and its influence on microstructural changes in C-Mn steel and vanadium microalloyed steel at the hot strip mill, ISIJ Int. 33 (1993) 605–614, https://doi.org/10.2355/isijinternational.33.605.
[46] P.D. Hodgson, R.K. Gibbs, A mathematical model to predict the mechanical properties of hot rolled C-Mn and microalloyed steels, ISIJ Int. 32 (1992) 1329–1338, https://doi.org/10.2355/isijinternational.32.1329.
[47] M.C. Somani, L.P. Karjalainen, A rationale for SRX regression model of hot-deformed austenite using an orthogonal Taguchi L8 matrix steels, Mater. Sci. Forum 715–716 (2012) 751–757, https://doi.org/10.4028/www.scientific.net/MSF.715-716.751.